Stratospheric influence on the seasonal cycle of nitrous oxide in the troposphere as deduced from aircraft observations and model simulations

Kentaro Ishijima,[1] Prabir K. Patra,[1] Masayuki Takigawa,[1] Toshinobu Machida,[2] Hidekazu Matsueda,[3] Yosuke Sawa,[3] L. Paul Steele,[4] Paul B. Krummel,[4] Ray L. Langenfelds,[4] Shuji Aoki,[5] and Takakiyo Nakazawa[1,5]

Received 2 October 2009; revised 25 June 2010; accepted 9 July 2010; published 27 October 2010.

[1] The atmospheric N_2O variations between the Earth's surface and the lower stratosphere, simulated by an atmospheric general circulation model–based chemistry transport model (ACTM), are compared with aircraft and satellite observations. We validate the newly developed ACTM simulations of N_2O for loss rate and transport in the stratosphere using satellite observations from the Aura Microwave Limb Sounder (Aura-MLS), with optimized surface fluxes for reproducing N_2O trends observed at the surface stations. Observations in the upper troposphere/lower stratosphere (UT/LS) obtained by the Japan AirLines commercial flights commuting between Narita (36°N), Japan, and Sydney (34°S), Australia, have been used to study the role of stratosphere-troposphere exchange (STE) on N_2O variability near the tropopause. Low N_2O concentration events in the UT region are shown to be captured statistically significantly by the ACTM simulation. This is attributed to successful reproduction of stratospheric air intrusion events and N_2O vertical/horizontal gradients in the lower stratosphere. The meteorological fields and N_2O concentrations reproduced in the ACTM are used to illustrate the mechanisms of STE and subsequent downward propagation of N_2O-depleted stratospheric air in the troposphere. Aircraft observations of N_2O vertical profile over Surgut (West Siberia, Russia; 61°N), Sendai-Fukuoka (Japan; 34°N–38°N), and Cape Grim (Tasmania, Australia; 41°S) have been used to estimate the relative contribution of surface fluxes, transport seasonality in the troposphere, and STE to N_2O seasonal cycles at different altitude levels. Stratospheric N_2O tracers are incorporated in the ACTM for quantitative estimation of the stratospheric influence on tropospheric N_2O. The results suggest strong latitude dependency of the stratospheric contribution to the tropospheric N_2O seasonal cycle. The periods of seasonal minimum in the upper troposphere, which are spring over Japan and summer over Surgut, are in good agreement between the ACTM and observation and indicate a different propagation path of the stratospheric signal between the two sites in the Northern Hemisphere. The stratospheric tracer simulations, when utilized with the observed seasonal cycle, also provide qualitative information on the seasonal variation in surface fluxes of N_2O.

Citation: Ishijima, K., et al. (2010), Stratospheric influence on the seasonal cycle of nitrous oxide in the troposphere as deduced from aircraft observations and model simulations, *J. Geophys. Res.*, *115*, D20308, doi:10.1029/2009JD013322.

[1]Environmental Biogeochemical Cycle Research Program, Research Institute for Global Change, Agency for Marine-Earth Science and Technology, Yokohama, Japan.
[2]Global Environmental Research Center, National Institute for Environmental Studies, Tsukuba, Japan.
[3]Geochemical Research Department, Meteorological Research Institute, Tsukuba, Japan.
[4]Centre for Australian Weather and Climate Research, CSIRO Marine and Atmospheric Research, Aspendale, Victoria, Australia.
[5]Center for Atmospheric and Oceanic Studies, Tohoku University, Sendai, Japan.

0148-0227/10/2009JD013322

1. Introduction

[2] Nitrous oxide (N_2O) in the atmosphere acts as the third most significant anthropogenically produced greenhouse gas and also has a dominant role in stratospheric ozone depletion [*Crutzen*, 1970; *Forster et al.*, 2007; *Ravishankara et al.*, 2009]. The atmospheric N_2O concentration is still increasing at an average rate of 0.2% yr^{-1}, even though efforts to mitigate N_2O emissions continue under the United Nations Framework Convention on Climate Change (UNFCCC) and the Kyoto Protocol. N_2O sources consist of both natural emissions (~11 TgN yr^{-1}, soil: ~60%,

ocean: ~35% and atmospheric chemistry (NH_3 oxidation): ~5%), and anthropogenic emissions (~6.7 TgN yr^{-1}), in which agriculture is the largest (~2.8 TgN yr^{-1}) mostly due to use of nitrogen fertilizers [*Forster et al.*, 2007]. Of this total source, ~12.5 TgN yr^{-1} of N_2O is destroyed by photolysis due to solar ultraviolet radiation and reaction with O (^1D) in the stratosphere (Tg = 10^{12} g). However, the estimates of N_2O sources and sinks remain largely uncertain, for both the regional as well as sectoral emission strength. For example, the best estimates of ratio of Northern to Southern Hemisphere (NH/SH) emissions still have a large range of 1.5–2.7 [*Butler et al.*, 1989; *Prinn et al.*, 1990; *Bouwman et al.*, 1995; *Hirsch et al.*, 2006; *Huang et al.*, 2008]. The source uncertainty is mainly due to lack of sufficient observations of N_2O fluxes across the land/ocean-atmosphere interfaces as well as large spatiotemporal variabilities of the fluxes.

[3] In order to monitor trends in the global N_2O budget, use of direct atmospheric concentration measurements is currently the most reliable approach. The measurement precision for N_2O has been improving gradually because of developments in gas chromatography (GC) components, such as the detector, oven and column, since the early measurements of the atmospheric N_2O concentration [*Weiss*, 1981]. Improvements in measurement techniques and an increase in the observation network density have allowed the derivation of long-term trends, seasonal cycle and interannual variation of the atmospheric N_2O concentration [*Prinn et al.*, 1990, 2000; *Ishijima et al.*, 2001, 2009; *Levin et al.*, 2002; *Liao et al.*, 2004; *Jiang et al.*, 2007; *Nevison et al.*, 2007]. The seasonal amplitude is at most only 0.3% (~1 ppb) of the absolute N_2O concentration at surface sites in the troposphere [*Jiang et al.*, 2007]. This places stringent demands on making very precise measurements (repeatabilities of 0.1% or better) to allow the seasonal cycle to be discerned and its amplitude quantified so that this information can be used to help identify the causes of seasonal N_2O variations. Recently N_2O surface fluxes have been estimated by inverse modeling methods using atmospheric N_2O measurements at a network of sites and forward CTM simulations, where a large estimation uncertainty often resulted from model N_2O transport, particularly due to STE [*Hirsch et al.*, 2006; *Huang et al.*, 2008].

[4] In addition to tropospheric measurements of N_2O, global observations of stratospheric N_2O with sensors onboard satellites have also been developed since the end of the 1970s (Nimbus7-SAMS [*Jones and Pyle*, 1984]). At present, higher-quality retrieval of N_2O is possible by advanced sensors such as the Aura-MLS [*Lambert et al.*, 2007], Odin-SMR [*Urban et al.*, 2005] and SCISAT–1-ACE-FTS [*Strong et al.*, 2008]. These data are useful to understand the stratospheric N_2O variabilities and evaluate the representation of N_2O loss processes in the CTM, but are not of the quality required for studying variations in tropospheric N_2O as the retrieval error increases toward the UT/LS region from the upper stratosphere. Most recently, systematic measurements of N_2O and other trace gases along horizontal transects are being made from flask samples of air collected on board commercial aircraft at regular intervals in the UT/LS region [*Matsueda et al.*, 2008; *Schuck et al.*, 2010]. Vertical profiles of trace gas composition (including N_2O) through all or much of the troposphere have also been carried out by flying aircraft at regular intervals over fixed sites [*Francey et al.*, 1999; *Ishijima et al.*, 2001; *Machida et al.*, 2001].

[5] Stratosphere-troposphere exchange (STE) is recently thought to be contributing significantly to the N_2O seasonal minima near the Earth's surface in summer to autumn in northern mid to high latitudes [*Levin et al.*, 2002; *Nevison et al.*, 2004; *Liao et al.*, 2004], despite the land surface fluxes peaking in this season due to enhanced microbial activities in both natural and agricultural soils [*Bouwman et al.*, 1995; *Potter et al.*, 1996]. *Nevison et al.* [2004] performed CTM simulations of N_2O and CFCs to show that these species' concentrations near the Earth's surface are significantly affected by intrusions of (N_2O and CFC depleted) stratospheric air which develops in early spring near the tropopause and propagates down to the surface with several months lag [e.g., *Liang et al.*, 2009]. This stratospheric influence thus has a measurable impact on the global budget of N_2O, for example, in the estimation of surface N_2O fluxes by top-down approaches. *Huang et al.* [2008] suggested that use of N_2O measurements in the UT/LS region, in comparison with CTM simulations is required to validate the estimation of the STE effect on tropospheric N_2O, and enable the estimation of seasonal and interannual variations of N_2O surface fluxes more accurately by inverse modeling methods.

[6] In this paper, we validate ACTM N_2O variations in the UT/LS region using several sets of aircraft observation data as well as latitude-pressure distributions from Aura-MLS satellite observations in the stratosphere. We have also estimated the vertical profile of the stratospheric influence on the tropospheric N_2O seasonal cycle, from vertical profile measurements at three aircraft observation sites and simulations of newly defined stratospheric tracers. For this purpose, the altitude range from the stratosphere to the Earth's surface has been explored extensively by using tropospheric aircraft observations and ACTM forward simulations of N_2O.

2. Description of Observation Data and Model

2.1. Observation Data

[7] To validate the ACTM simulations for atmospheric N_2O concentration in the lower stratosphere regions, we use data from Microwave Limb Sounder on board the Aura satellite (Aura-MLS) [*Lambert et al.*, 2007]. Aircraft observations in the UT/LS region over the western Pacific are used to evaluate the model performance in terms of simulating the STE of atmospheric N_2O. These measurements are conducted by the National Institute for Environmental Studies (NIES), Meteorological Research Institute (MRI) and Japan Airlines, as a part of the Comprehensive Observation Network for TRace gases by AIrLiner (CONTRAIL) since December 2005 [*Machida et al.*, 2008; *Matsueda et al.*, 2008]. Between Narita (36°N, 140°E), Japan and Sydney (34°S, 151°E), Australia, 12 air samples are collected fortnightly in metal flasks using the Automatic Air Sampling Equipment (ASE) [*Matsueda et al.*, 2008] in the altitude range of 9–11 km (Figure 3) between 32°N and 30°S at 5.6 degrees intervals as shown in Figure 1. The samples are analyzed at NIES using a gas chromatograph (GC) equipped with an electron capture detector (ECD) for

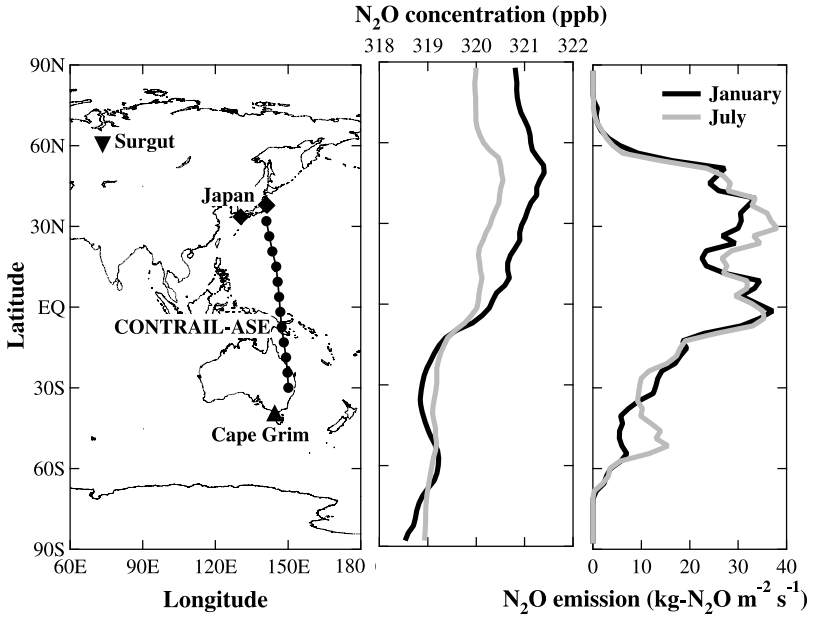

Figure 1. (left) Locations of aircraft observation sites used in this study. Latitudinal distributions of monthly means of N_2O concentration at the surface, (middle) averaged across all longitudes and N_2O emission and (right) averaged across all longitudes in January and July 2006, derived from the ACTM simulations. Both distributions are averaged for each latitude of the model grid (T42 Gaussian latitude: ~2.8° intervals).

N_2O concentration. The samples are also analyzed for several other species and their isotopic ratios. To assess seasonal variations of tropospheric N_2O, we also use observation data sets at monthly intervals from three aircraft-borne flask sampling sites: (1) Surgut, West Siberia, Russia (61°N, 73°E) at altitudes of 0.5, 1.0, 1.5, 2.0, 3.0, 4.0, 5.5 and 7.0 km by NIES for the period April 2001 to February 2005 using chartered aircraft [*Nakazawa and Sugawara*, 1997; *Machida et al.*, 2001]; (2) Sendai, Japan (38°N, 141°E), below 4 km altitude using chartered aircraft and by Japan AirLines (JAL) commercial airliners regularly commuting between Sendai and Fukuoka, Japan (34°N, 130°E), at altitudes between 4 and 11 km, by Tohoku University [*Nakazawa et al.*, 1993; *Ishijima et al.*, 2001] for the period June 2001 to November 2008; and (3) Cape Grim, Tasmania, Australia (41°S, 145°E), between 0.15 km and 8 km by Commonwealth Scientific and Research Organization (CSIRO) for the period September 1992 to September 2000 [*Francey et al.*, 1999, 2003]. Locations of these widely separated aircraft observation sites are also shown in Figure 1.

2.2. ACTM Chemistry Setup

[8] We have used the Center for Climate System Research/National Institute for Environmental Studies/Frontier Research Center for Global Change atmospheric general circulation model (CCSR/NIES/FRCGC AGCM) [*Numaguti et al.*, 1997] with chemical reactions (which we refer to as the ACTM) for simulations of atmospheric N_2O. Details of the current ACTM version and subgrid to interhemispheric scale transport representations are described by *Patra et al.* [2009a]. Estimates of the interhemispheric exchange time (~1.3 years) calculated using SF_6 observations and ACTM simulations agree within 10%. The horizontal and vertical resolution of the model are T42 spectral truncation (~2.8 × 2.8°) and 67 sigma-pressure vertical layers (surface to about 90 km), respectively. The model transport is nudged toward NCEP/DOE AMIP-II reanalysis [*Kanamitsu et al.*, 2002] (ftp.cdc.noaa.gov:/Data sets/ncep.reanalysis2/spectral) horizontal winds and temperature at 6 hourly time intervals. N_2O losses consisting of photolysis by solar ultraviolet (UV) radiation and two kinds of oxidation reactions with $O(^1D)$ in the stratosphere are incorporated. The loss reactions and rate constants used in ACTM are as follows:

$$\text{(R1)} \qquad N_2O + UV \rightarrow N_2 + O(^1D),$$

$$\text{(R2a)} \qquad N_2O + O(^1D) \rightarrow 2NO\left(K_a = \left(6.7 \times 10^{11}\right) \times EXP(20/T)\left[cm^3\ molecule^{-1}s^{-1}\right]\right),$$

$$\text{(R2b)} \qquad N_2O + O(^1D) \rightarrow N_2 + O_2\left(K_b = \left(4.7 \times 10^{11}\right) \times EXP(20/T)\left[cm^3\ molecule^{-1}s^{-1}\right]\right).$$

Here, T is the air temperature for each model grid. Absorption cross sections of N_2O used in (R1) and the rate constants used in (R2a) and (R2b) are taken from the JPL synthesis report [*Sander et al.*, 2006]. The N_2O photolysis rate (J_{N2O}) is calculated for three wavelength ranges of 185–200 nm, 200–230 nm and 230–278 nm, and the temperature dependency of the absorption cross sections is considered. The radiation transfer calculation scheme to provide actinic flux for the photolysis rate calculation is developed by *Sekiguchi and Nakajima* [2008]. The concentration of $O(^1D)$ is calculated online in the ACTM using a climatological ozone

Table 1. Combination of Annual Mean Anthropogenic and Natural Soil Fluxes, and Monthly Mean Ocean Fluxes of N_2O, and the NH/SH Ratio of the Emissions in the Best Scenario for the Year 2000[a]

		Emission (Best Guess)		Emission Range (All 27 Cases)	
Source Type	Inventory Source	Annual Total (Tg-N yr^{-1})	NH/SH Ratio	Annual Total (Tg-N yr^{-1})	NH/SH Ratio
Anthropogenic	EDGAR 3.2 FT2000	7.3	4.3	7.3–7.5	4.3
Natural Soil	EDGAR 2.0 × 1.14	7.5	1.3	6.2–7.5	1.3–1.5
Ocean	*Nevison et al.* [1995]	3.6	0.75	3.6–9.9	0.75
Total		18.5	1.74	18.5	1.3–2.0

[a]The emission ranges for all 27 scenarios used in test simulations are also given. A scaling factor of 1.14 is applied to the soil emission by EDGAR 2.0 only.

distribution, and the ozone photolysis rate in the above wavelength ranges at each model grid [*Takigawa et al.*, 1999]. We have neglected the N_2O production reaction $N_2 + O(^1D) + M \rightarrow N_2O$ [*Sander et al.*, 2006], because the production rate has been estimated to be about 5 orders of magnitude less than that of N_2O loss in the stratosphere in our model. Mean atmospheric lifetime of N_2O in the ACTM is 101 years for the period 1993–2007, which is shorter than the IPCC recommended value of 114 years [*Forster et al.*, 2007]. This is mainly caused by a little too fast Brewer-Dobson (B-D) circulation in ACTM. For example, the air age in the ACTM is up to 40% and 20% younger at 20 and 25 km, respectively, than that calculated from the balloon-borne observations of CO_2 over Sanriku, Japan (39°N, 142°E) [*Aoki et al.*, 2003], but is fairly consistent above 30 km. To obtain realistic trends of global radiation budgets in the model, carbon dioxide (CO_2) and methane (CH_4) are also simultaneously calculated using realistic surface fluxes and chemical reactions [*Patra et al.*, 2008, 2009b]. Details on calculations of these components and general features of dynamical aspects of chemical tracer transport in this model are described by *Takigawa et al.* [1999] and *Patra et al.* [2008, 2009a, 2009b].

2.3. Emission Scenarios

[9] We combined three source categories of N_2O flux for simulations in this study, i.e., natural soils, the oceans and an anthropogenic flux. Annual mean natural soil fluxes of N_2O are taken from the Emission Database for Global Atmospheric Research (EDGAR; version 2.0 [*Bouwman et al.*, 1993], http://www.mnp.nl/edgar), and scaled by a factor of 1.14 (as discussed at the end of this section). For oceanic emissions, monthly varying fluxes by *Nevison et al.* [1995] are used. For anthropogenic fluxes, annual mean fluxes from EDGAR 32 (version 3.2 [*Olivier et al.*, 2005], http://www.rivm.nl/edgar/model) are employed. These three source types were selected based on 27 test scenarios (Table 1). Oceanic fluxes by *Nevison et al.* [1995], natural soil fluxes by EDGAR 2 and the Carnegie Ames Stanford Approach (CASA) terrestrial ecosystem model [*Potter et al.*, 1996] (ftp://talon.arc.nasa.gov/pub/glemis), anthropogenic fluxes by EDGAR 32, and land fluxes by *Bouwman et al.* [1995] were combined to prepare the 27 different flux combinations. To make each emission scenario by combining three source types, only one source type was scaled by a factor to preserve global total flux, thus maintaining the simulated N_2O trend at the observed level. Details of the best scenario selected for reproducing the latitudinal distribution and seasonal cycle of observed atmospheric N_2O concentration, along with the emission ranges for all 27 scenarios, are given in Table 1. The latitudinal distribution of N_2O emissions in the best scenario for January and July 2006 and corresponding ACTM simulation results are shown in Figure 1. The simulated N_2O interhemispheric gradient of around 1.5 ppb compares well with the observed value (as in work by *Huang et al.* [2008]). The NH/SH ratio of N_2O emissions for our best case is 1.75 ± 0.5 for the period 1990–2007, supporting the early results by *Butler et al.* [1989] and *Prinn et al.* [1990].

[10] For anthropogenic fluxes before 2000, the EDGAR 32 inventories for 1990 and 1995, and EDGAR 32FT2000 are interpolated linearly for each source category, and then combined to prepare total anthropogenic fluxes corresponding to each year. The emission scenario after 2000 was decided by a simulation using 10 different anthropogenic emission scenarios with the same spatial distribution as that of EDGAR 32FT2000, but with different linear trends resulting in 1.00–1.07 times the EDGAR 32FT2000 emission in 2010. The scenario with 1.035 times emission EDGAR 32FT2000 in 2010 was selected as the best for ACTM to reproduce the global average N_2O concentration as observed. We used monthly averaged values of continuous N_2O observations from Mace Head (Ireland), Trinidad Head (California, USA), Ragged Point (Barbados), Cape Matatula (American Samoa), Cape Grim (Tasmania, Australia) by Advanced Global Atmospheric Gases Experiment (AGAGE; http://agage.eas.gatech.edu/stations.htm), and from Point Barrow (Alaska, USA) and South Pole by National Oceanic and Atmospheric Administration/Earth System Research Laboratory/Global Monitoring Division (NOAA/ESRL/GMD; http://www.esrl.noaa.gov/gmd/). Annual total emissions of 18.2, 18.5 and 18.6 Tg-N yr^{-1} in 1990, 2000 and 2005, respectively, are used in the ACTM simulation. This emission trend is likely to reflect a real N_2O emission trend, but the annual totals are probably overestimated due to the relatively short lifetime of N_2O in ACTM (section 2.2).

2.4. Model Run

[11] We have run the model for the period January 1979 to January 2008, and simulation results after 1992 are used for this study. The simulation prior to 1992 is treated as a spin-up period for N_2O photochemistry and atmospheric transport. The spin-up for 13 years is considered sufficient, because the simulation is started with realistic vertical and horizontal N_2O gradients. The local lifetimes of N_2O are several decades, a few years and less than half year, just above the tropical tropopause, around 25 km and over 30 km in the stratosphere, respectively. The modeled N_2O concentrations are readjusted to observed values for January 1989 before starting the latter half of the simulation.

2.5. Stratospheric Tracer

[12] In order to separate the stratospheric influences on N_2O concentration variations in the troposphere, we have incorporated hypothetical stratospheric tracers in the ACTM, which are defined as follows:

[13] 1. The simulated N_2O for the best emission case (hereafter called "normal N_2O") above the tropopause is defined as "stratospheric tracer" (hereafter called "ST").

[14] 2. Another stratospheric tracer is defined in the same manner as (1), but the tracer's concentration above the tropopause is the same as normal N_2O concentration in the troposphere (hereafter called "STT"). At each time step, ST concentration above the tropopause is replaced by normal N_2O concentration in the stratosphere, while STT concentration above the tropopause is replaced by normal N_2O concentration in the troposphere.

[15] 3. Fractions of the above two hypothetical tracers are transported into the troposphere through STE processes. The amount of STT transported into the troposphere is slightly larger than that of ST, because STT has the tropospheric concentration above the tropopause, which is always higher than the stratospheric concentration (Figure 2 and 4).

[16] 4. (ST-STT) in the troposphere is defined as the stratospheric contribution to the tropospheric N_2O concentration (e.g., to see the stratospheric influence at the altitude of 3 km, the STT whose concentration above the tropopause is that at the altitude of 3 km is used). Note that a larger amount of STT in the troposphere has larger "negative" effect on the tropospheric N_2O concentration.

[17] 5. (ST-STT) is negative in most cases, but the stratospheric effect on seasonal variation of the tropospheric N_2O concentration is deviation of (ST-STT) from its annual mean.

[18] A spin-up period for the stratospheric tracers is from January 1991 to the beginning of the aircraft observation over Cape Grim (September 1992). The period of 1.7 years is very short compared to the N_2O lifetime, but roughly enough because they have to circulate mainly in the troposphere. Growth rates of the stratospheric tracers are about half of that of the normal N_2O for the period 1993–2008.

[19] The above procedure is based on an assumption that if the N_2O concentration is vertically homogeneous throughout both the troposphere and stratosphere, there would be no stratospheric effect on the tropospheric N_2O. However, in reality the N_2O concentration is lower in the stratosphere than in the troposphere. Therefore, we regard the propagation of (ST-STT) from the stratosphere into the troposphere, as the stratospheric effect on the tropospheric N_2O. This concept is different from that used in previous studies [e.g., *Sudo and Akimoto*, 2007; *Liang et al.*, 2009], since we do not directly use concentration values of the "stratospheric tracer."

[20] The tropopause height is determined in the ACTM using the definition by the World Meteorological Organization (WMO) of the temperature lapse rate of -2 K km^{-1}. Tropopause heights determined by the ACTM are shown in Figure 4, and are generally consistent with the height of large changes in the vertical N_2O gradient. The sensitivity of the tropopause height to lapse rate in ACTM is on the order of 0.5 km for a change of 1 K km^{-1} in lapse rate. Depending on the tropopause height, the amount of the stratospheric tracer entering the troposphere would change, since the normal N_2O above the tropopause becomes the stratospheric tracer every time step in ACTM. However, the stratospheric contribution to the N_2O seasonal cycle is not very sensitive to the tropopause height in our test simulations because the differences between two stratospheric tracers are used.

2.6. Model Sampling and Data Analysis

[21] For comparisons with observations, model results at the same time and location as those of the observations are extracted by four-dimensional linear interpolation of the model output (along longitude, latitude, pressure sigma, and time axes). In the case of CONTRAIL-ASE, the time and latitude/longitude of sampling are recorded precisely. The time and sampling locations over Surgut and Japan are recorded at accuracy of several hours and of 0–2 degrees in latitude/longitude, respectively. Therefore, hourly snapshot outputs of model results are used for comparison with CONTRAIL-ASE, while daily mean outputs are used for aircraft observations of vertical profiles at three sites.

[22] For calculating N_2O seasonal cycles at the three vertical profile observation sites, we applied the digital filtering technique of *Nakazawa et al.* [1997] to the time series, after grouping the data at 1 km intervals. The observation data are represented by the following fitted curve,

$$B(t) = L(t) + S(t) + I(t),$$

where B(t) is the best fit curve, L(t) is the long-term trend, which is calculated by passing the observation data (O(t)) through a low-pass filter with a cutoff period of 36 months, S(t) is the average seasonal cycle component, which is obtained by fitting a Fourier function of 3 harmonics with 12, 6 and 3 months period to O(t)-L(t), and I(t) is the irregular component, which is obtained by passing O(t)-L(t)-S(t) through a low-pass filter with a cutoff period of 4 months. In this study, we calculate monthly means of S(t)+I(t) to represent the mean seasonal cycle and the standard deviation.

3. Results

3.1. N_2O in the Stratosphere: Validation Using MLS Observations

[23] We first compare our model results with the Aura-MLS satellite observations to validate N_2O concentration in the lower stratosphere regions, before focusing on the tropospheric distribution of N_2O. Figure 2 shows monthly and zonal mean latitude-pressure cross sections of N_2O observed by Aura-MLS and simulated by ACTM. The MLS data between 100 and 1 hPa are used, following the recommendations by *Lambert et al.* [2007]. For comparing with MLS data, model simulations at the same latitude/longitude/pressure-level/time as those of each MLS data value are extracted from hourly snapshot outputs. Both MLS and ACTM show a decrease in concentration from low to high latitudes, and the lower to upper stratosphere altitude range (100 to 1 hPa) in a fairly similar way. It is known that MLS has negative bias below 50 hPa especially in the tropics [*Lambert et al.*, 2007], which is also appearing in this figure. Upon entry into the stratosphere, through the tropical upwelling branch of the Brewer-Dobson circulation, N_2O is

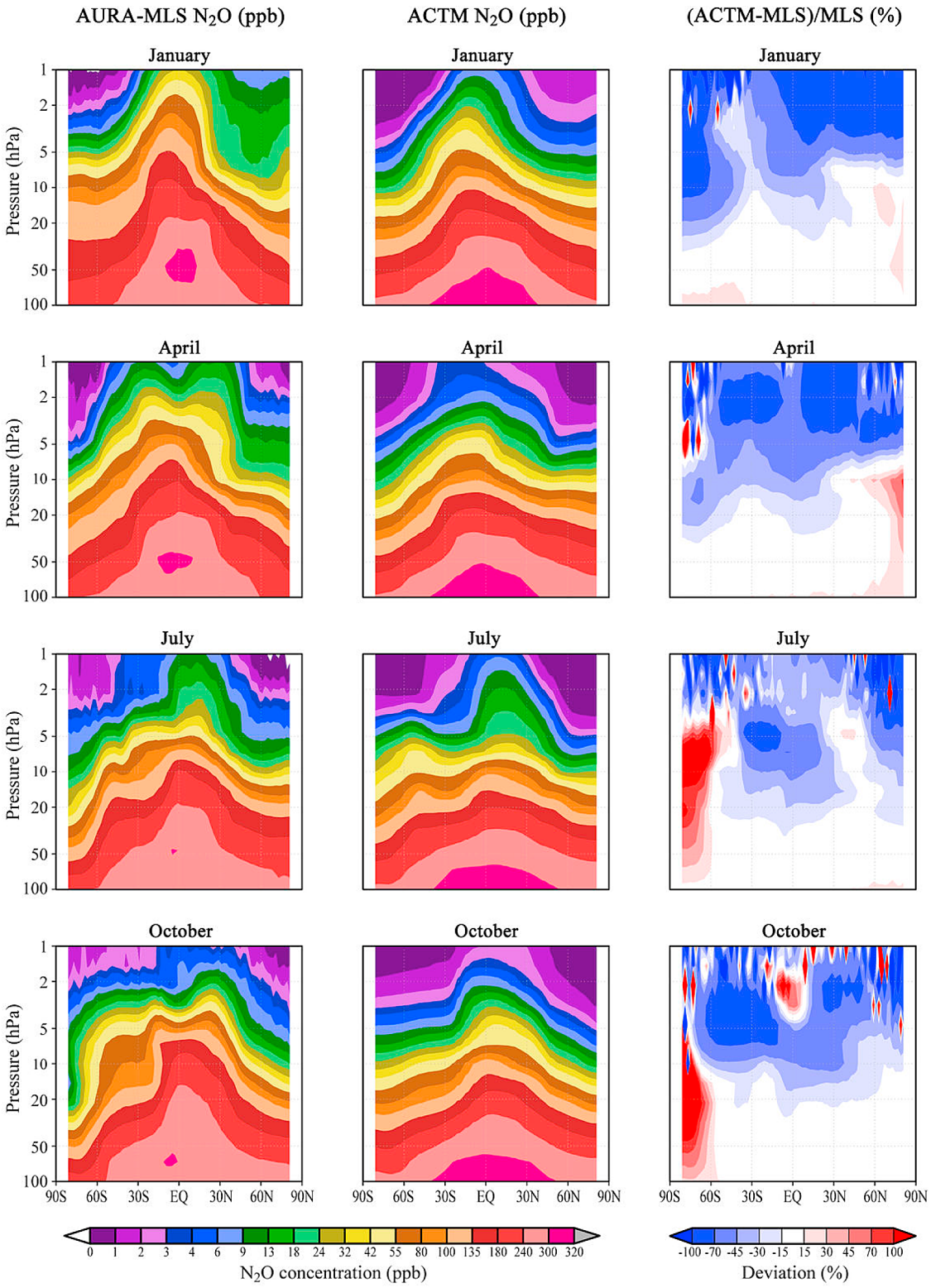

Figure 2. Monthly zonal mean N_2O concentration (left) observed by Aura-MLS and (middle) simulated by the ACTM in January, April, July, and October in 2006, together with (right) the deviation (in percentage) of the ACTM simulated values from those of Aura-MLS, normalized by the Aura-MLS values.

transported to the Northern Hemisphere (NH) during July–October and to the Southern Hemisphere (SH) during January–April. These features appear well in both MLS observations and ACTM simulations. The ACTM tends to overestimate N_2O concentrations in polar regions compared to the MLS observations, which is seen more prominently over Antarctica in October in Figure 2 (up to about 100%). This behavior is thought to be arising mainly from deficient

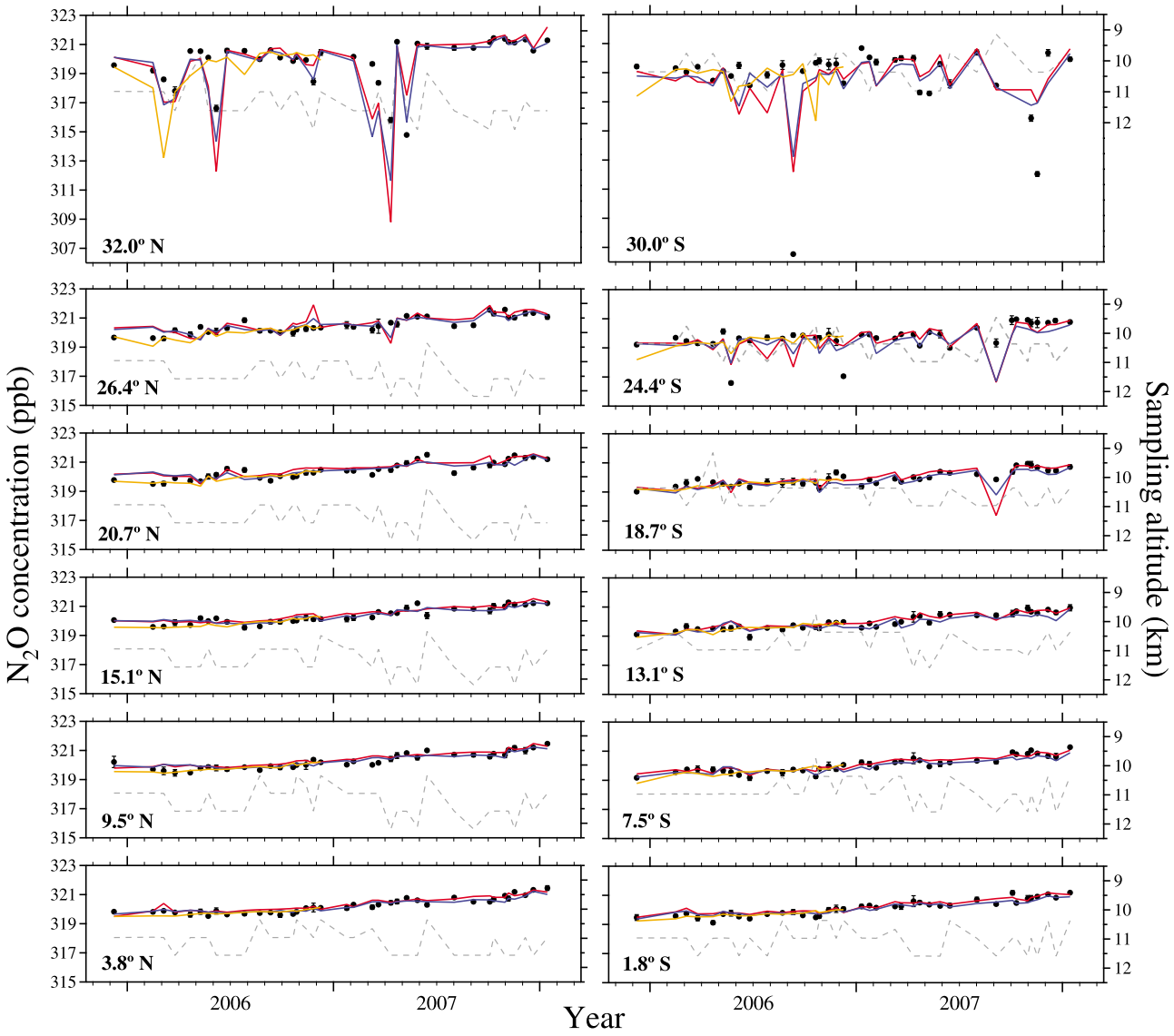

Figure 3. N_2O concentration at each latitude obtained by CONTRAIL-ASE observation (dot) and simulated by the ACTM (red line). The ACTM results simulated with the Japanese 25 year ReAnalysis (JRA-25) data from the Japan Meteorological Agency (JMA) (JRA-25, blue line) and without nudging (free run, yellow line) are also shown. Also, each air sampling altitude is shown by the gray dashed lines (note, the sampling altitude scale on the right axis is shown as reversed).

polar vortex isolation from mixing with mid latitude air, due to the relatively low horizontal model resolution (T42). Low wavelength resolution in the photolysis rate calculation may partly be responsible for the N_2O overestimation in the polar region (see section 2.2). The differences between results from the MLS and the ACTM are shown in Figure 2 (right) (deviation of ACTM from MLS, normalized by MLS value). The ACTM simulation generally underestimates N_2O above 10 hPa. The tendency of the underestimation is similar to other model results [e.g., *Jin et al.*, 2009]. However, the ACTM results never become less than half (i.e., 100% in difference) of those by MLS at 1 hPa pressure level. In the lower stratosphere (below 30 hPa), the ACTM and MLS values agree within about 15% in all seasons except over Antarctica. This can be viewed as remarkable, considering the accuracy of MLS observations is estimated to be 13–25% for the 100–68 hPa levels [*Lambert et al.*, 2007]. Note also that the N_2O concentration gradient in the lower stratosphere region is the most important to elucidate the stratospheric influences on N_2O in the troposphere through STE.

3.2. N_2O in the UT/LS Using ASE Observation

[24] Figure 3 shows N_2O concentration time series at different latitudes as obtained by CONTRAIL-ASE observations and simulated by the ACTM. To test the sensitivity of the ACTM to nudging of the meteorological data, simulations are also made with the Japanese 25 year ReAnalysis data from the Japan Meteorological Agency (JMA) (JRA-25) [*Onogi et al.*, 2007] for the period 2005–2006 and without nudging (free run) for the same period, in addition to the control simulations nudged to NCEP2 reanalysis. The ACTM

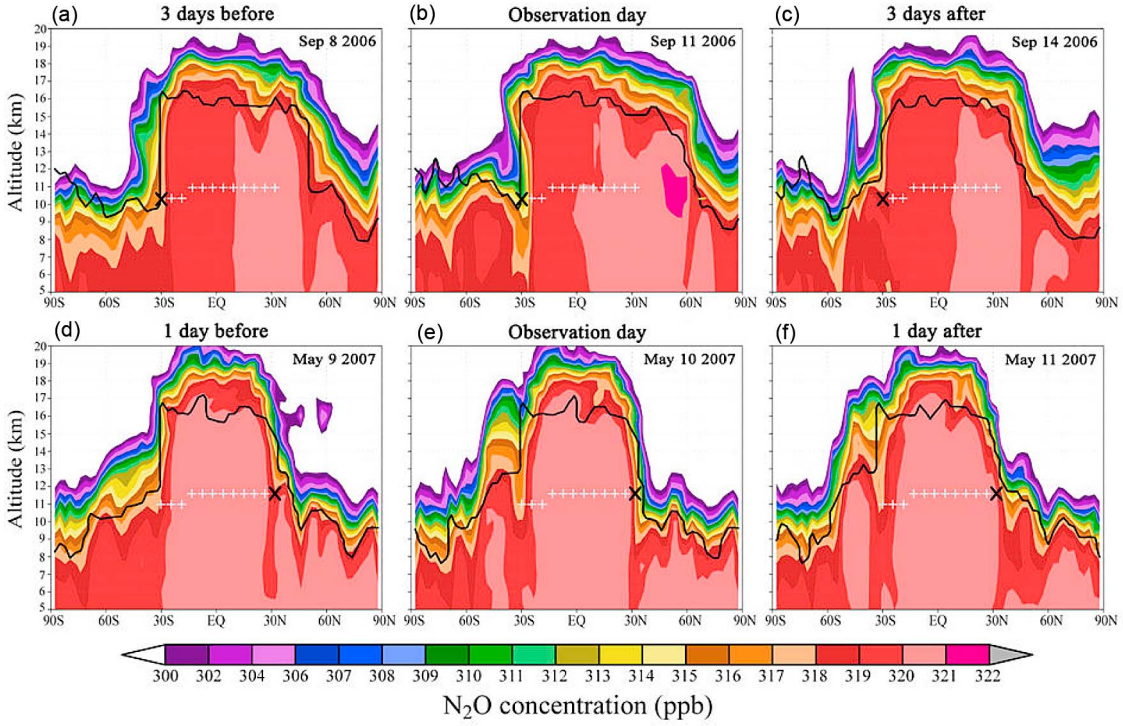

Figure 4. Snapshots of height-latitude cross sections of the ACTM N_2O concentration when the lowest N_2O concentrations were observed (b) at 30°S, 150°E on 11 September 2006 (observation day) and (e) at 32°N, 141°E on 10 May 2007 (observation day). The cross sections (a, d) before and (c, f) after the low concentration events (observation days) are also shown. Locations of the sampling points of the low N_2O events and at other latitudes are indicated by a cross and light-blue pluses, respectively, and the black solid lines indicate the position of the tropopause as judged by the ACTM. In both the case in September 2006 and May 2007, N_2O-depleted stratospheric air penetrates into the troposphere along with the tropopause descents, and then the region of low N_2O concentration dissipates within several days.

well simulates the N_2O growth rate at all latitudes, and also the occasional low concentrations seen only in the extratropics, especially at 32°N and 30°S. They are caused by intrusions of stratospheric air with low N_2O concentration from the tropopause break or due to tropopause folds or seasonal descent of the tropopause height during the winter to spring period in each hemisphere. The frequency of the low concentration events is slightly higher at 32°N in comparison to 30°S. It is known that wave activity originating from topography or cyclones is greater in the Northern Hemisphere compared to the Southern Hemisphere, which can lead to more frequent occurrence of STE events [e.g., *Holton et al.*, 1995; *Appenzeller et al.*, 1996; *Elbern et al.*, 1998].

[25] Figure 4 shows snapshots of latitude-altitude N_2O cross sections when the lowest concentration were observed at two selected sampling points of intense STE events that are consistently simulated by the ACTM. At the sampling point of 30°S, 150°E, from 8 to 11 September 2006, the stratospheric air has intruded along the isentropic surface of 320 K (Figures 4a and 4b). The fold pattern is very similar to that analyzed by *Baray et al.* [2000], which occurred in the southern subtropics associated with the descending branch of the Hadley circulation, accompanied by the convergent flow of stratospheric ozone into the troposphere. It is shown by the tropopause defined in the ACTM that the aircraft was almost completely in the stratospheric air at the time of flask sampling. This event has weakened after 3 days at 30°S, although another intensive one had evolved around 60°S (Figure 4c). At 32°N, 141°E, the aircraft encountered the edge of the tropopause lowering over 30°N–50°N, on 10 May 2007 (a stratospheric air intrusion at 30°S is also captured on this day as seen in both Figure 3 and Figure 4e. Descent of the tropopause height occurred over a shorter duration of a few days, compared to the case at 30°S which lasted for about a week. In addition to the different meteorological conditions that exist at 32°N and 30°S, there are also differences in air sampling altitudes, with those at 32°N typically 1 km higher than at 30°S (Figure 4).

[26] In Figure 3, the JRA-25 results are fairly consistent with the NCEP2 results, while the free-running model does not well reproduce either the timings or intensity of the low concentrations observed by the CONTRAIL-ASE. This indicates that nudging of the ACTM to meteorological data products, such as analysis or reanalysis, is required to better simulate the STE events, which strongly influence the N_2O variations in the UT/LS region.

[27] In Figure 5, the latitudinal distribution of N_2O in the UT/LS regions is captured extremely well, taking into account the average observational precision of 0.2 ppb, with the largest difference of only 0.4 ppb seen at 32°N. Standard deviations, calculated based on full time series data (December 2005 to January 2008), are also consistent between observations and the ACTM simulation, apart from

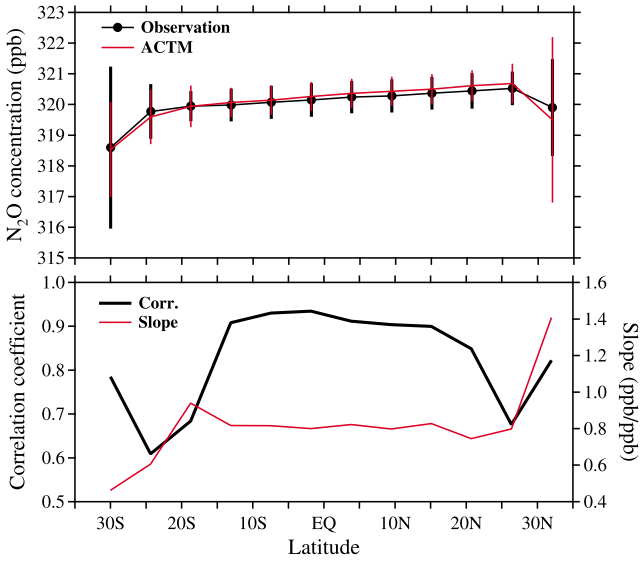

Figure 5. (top) Latitudinal distribution of mean N_2O concentration observed by CONTRAIL-ASE and simulated by the ACTM for the period from December 2005 to January 2008, together with the standard deviations. (bottom) Latitudinal distribution of correlation coefficient and slope (ACTM/observation) between the results (see text).

some differences seen at 32°N (overestimation by 1.1 ppb) and 30°S (underestimation by 1.0 ppb). At these two sampling points, N_2O is the most variable compared to the lower latitude points. Therefore, it seems difficult to completely reproduce individual concentration levels of temporally coarse-resolution data, which are observed once or twice a month. This is manifested in slopes of scatterplots between ACTM results and observations, which suggest the model overestimates (slope ~1.4) and underestimates (slope ~0.5) the variability around the long-term mean at 32°N and 30°S, respectively. These results could indicate that the ACTM overestimates STE in the Northern Hemisphere, mainly due to some model features. Other than fast B-D circulation (mentioned in section 2.2), the sigma-pressure vertical coordinate employed in the ACTM is also considered. In that coordinate system, mass variability at the surface, which is large especially at high mountain areas in the Northern Hemisphere, directly transmits to upper layers. The effect is possible to increase STE in the Northern Hemisphere. However, we cannot place too much reliance on these results as yet, because the slope values at 32°N and 30°S, both in the observations and the ACTM, are mostly determined by only a few low concentration values (Figure 3). For the tropical latitudes, the model generally underestimates the concentration variability. The slope and correlation coefficients contains both the variability (dominates toward the higher latitudes) and trends (dominates toward the equator) in the time series. The correlations are excellent (up to 0.9) near the equator, because the trends are well reproduced mainly by the emission trend in the model, being free from influence of the direct stratospheric air intrusion. The correlation coefficients are also high at about 30° latitude in each hemisphere (~0.8), compared to those at around 25° (0.6~0.7). The sampling points around 30° in the both hemispheres are located in the region of high stratospheric air intrusion events, while the regions around 25° are located in the boundary between the equator and the region of highest stratospheric influence. Therefore, the ACTM can well reproduce low concentrations around 30°, but cannot simulate the delicate concentration gradient around 25° latitude in each hemisphere. These results suggest spatio-temporally finer meteorological observation data in the UT/LS region as well as a finer resolution model may be of further benefit to the STE event simulations.

3.3. N_2O in the Troposphere Using Vertical Profile Observations at Three Sites

[28] Next, we analyzed the atmospheric N_2O time series measured at three aircraft vertical profile observation sites, namely, Surgut, Japan and Cape Grim. Figure 6 shows atmospheric N_2O concentrations observed over Japanese islands using two types of aircrafts operated in different altitude ranges, and ACTM results along with the best fit curves obtained by digital filtering. Above 7 km, and especially over 9 km, very low concentrations are seen periodically both in observation and ACTM simulations. The areas over the main Japanese islands, where this air sampling is done (Figure 1), are highly affected by stratospheric air, in a similar way to the case at 32°N (and 30°S) in the CONTRAIL-ASE observation. This region is well known for the frequent occurrence of tropopause folds, developing on the polar and subtropical jets [*Muramatsu et al.*, 1984; *Elbern et al.*, 1998]. In Figure 6, for the data above 7 km, the best fit curves do not fit the data as well (compared to those below 7 km), due to the greater scatter in the N_2O values caused by the greater impact of relatively undiluted N_2O-depleted stratospheric air. In spite of such cases, the digital filtering technique works well enough to estimate average seasonal behavior such as amplitude and the timing of minima and maxima, if applied to a statistically significant number of data points over several annual cycles. Here, we use data from three aircraft vertical profile observation programs, which had been carried on for more than three years, to discuss seasonal cycles and the stratospheric influences on them. Average seasonal cycles for 3–6 years are used in the discussions.

3.3.1. N_2O Seasonal Cycles Over Surgut

[29] Figure 7 shows July minima in N_2O seasonal cycle as observed over Surgut in the height range of 1.0–5.5 km, which is consistently simulated by the ACTM. The summer N_2O minima are consistent with other aircraft observation results over Siberia by *Levin et al.* [2002]. The stratospheric contributions suggest that these minima are mainly the result of a combined effect of the stratospheric influence (blue line) and increased vertical transport/mixing during the summer [*Patra et al.*, 2009a]. By applying the digital-filtering technique to the time series data of ACTM results for each grid, we show (Animation 1)[1] height-latitude cross section of the ACTM simulated seasonal cycle at 73°E (corresponding to the longitude of Surgut). The low values in the upper troposphere propagate downward to the lower troposphere in spring at 30°N–40°N, and then expand northward during summer. During this time, convection activity increases in the temperate/boreal Northern Hemi-

[1]Animations are available in the HTML.

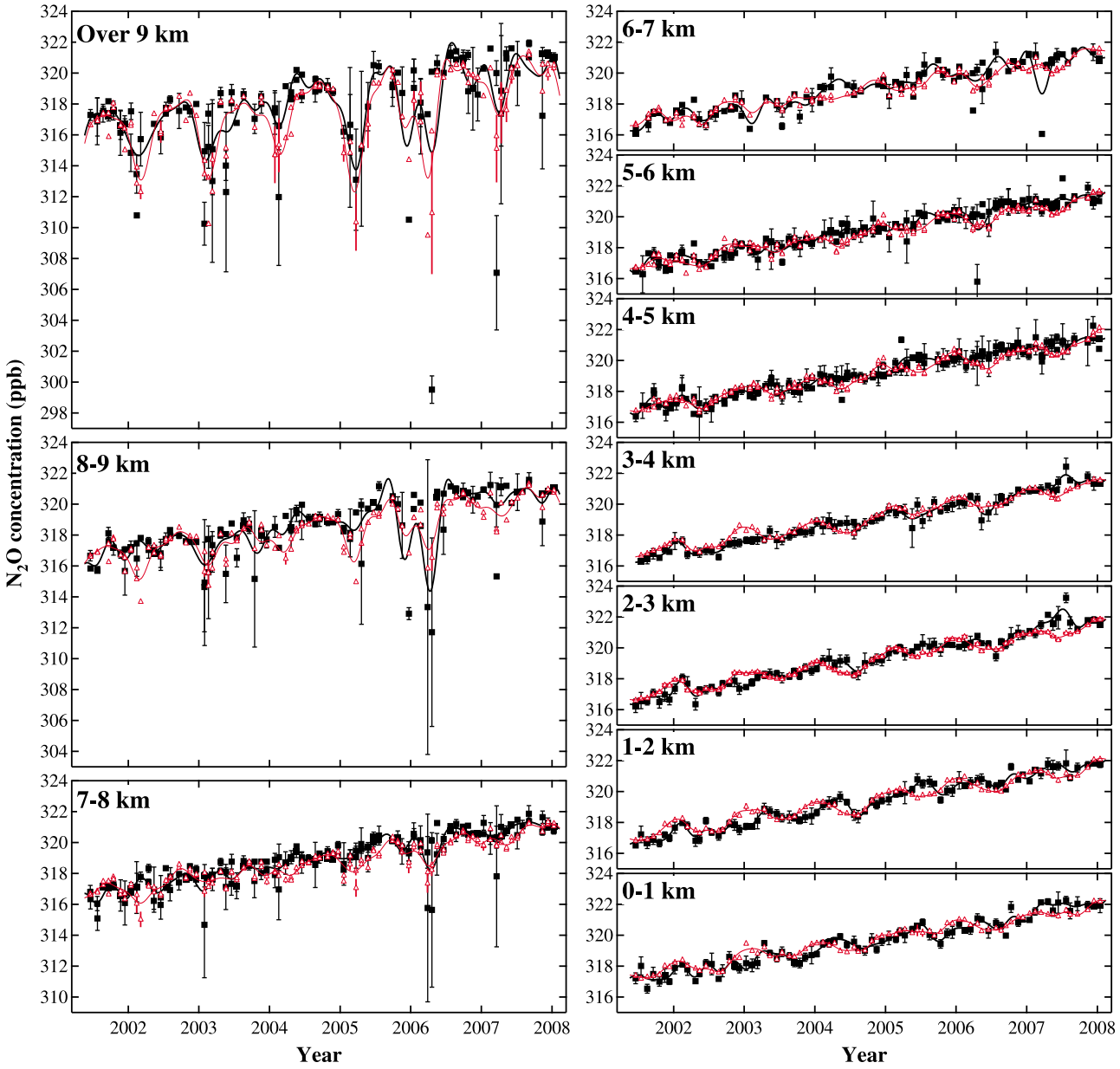

Figure 6. N_2O concentration at 0–1, 1–2, 2–3, 3–4, 4–5, 6–7, 7–8, 8–9, and over 9 km over Japan, observed by aircraft (black) and simulated by the ACTM (red). The aircraft observations have been performed below 4 km over Sendai (38°N, 141°E), Japan, and above 4 km on the route of the JAL commercial airliners between Sendai and Fukuoka (34°N, 130°E), Japan. Each symbol and error bar represents daily mean and its 1 standard deviation, respectively. Solid line represents the best fit curve calculated by a digital-filtering technique (see text).

sphere and promotes the vertically homogeneous N_2O concentration over Surgut compared to the winter season (see Figure 8).

[30] The location of maximum STE of N_2O in the latitude region of 30°N–40°N is in contrast with the maximum tracer STE occurring at 50°N–60°N latitude by *Liang et al.* [2009]. Their result is based on stratospheric tracers with lifetimes on the order of months, and fixed concentrations in the stratosphere. This condition creates strong tracer concentration gradients between the tropopause and the surface as opposed to the N_2O vertical distribution in the troposphere, exhibiting a rather constant value (within ~1 ppb). In contrast, the stratospheric N_2O significantly varies with season and latitude, but has no loss in the troposphere (Figure 2). Therefore, it is suggested that the location of strongest STE may vary with spatiotemporal distributions of tracers in the stratosphere and the lifetime in the troposphere.

[31] For verification of the stratospheric influence, we have also performed a simulation without the stratospheric chemical loss (not shown here), which produced N_2O seasonal amplitudes less than half of observed amplitudes at 1.5–5.5 km height over Surgut. However, the ACTM overestimates the stratospheric contribution in spring at 7 km, producing the largest model-observation mismatch at

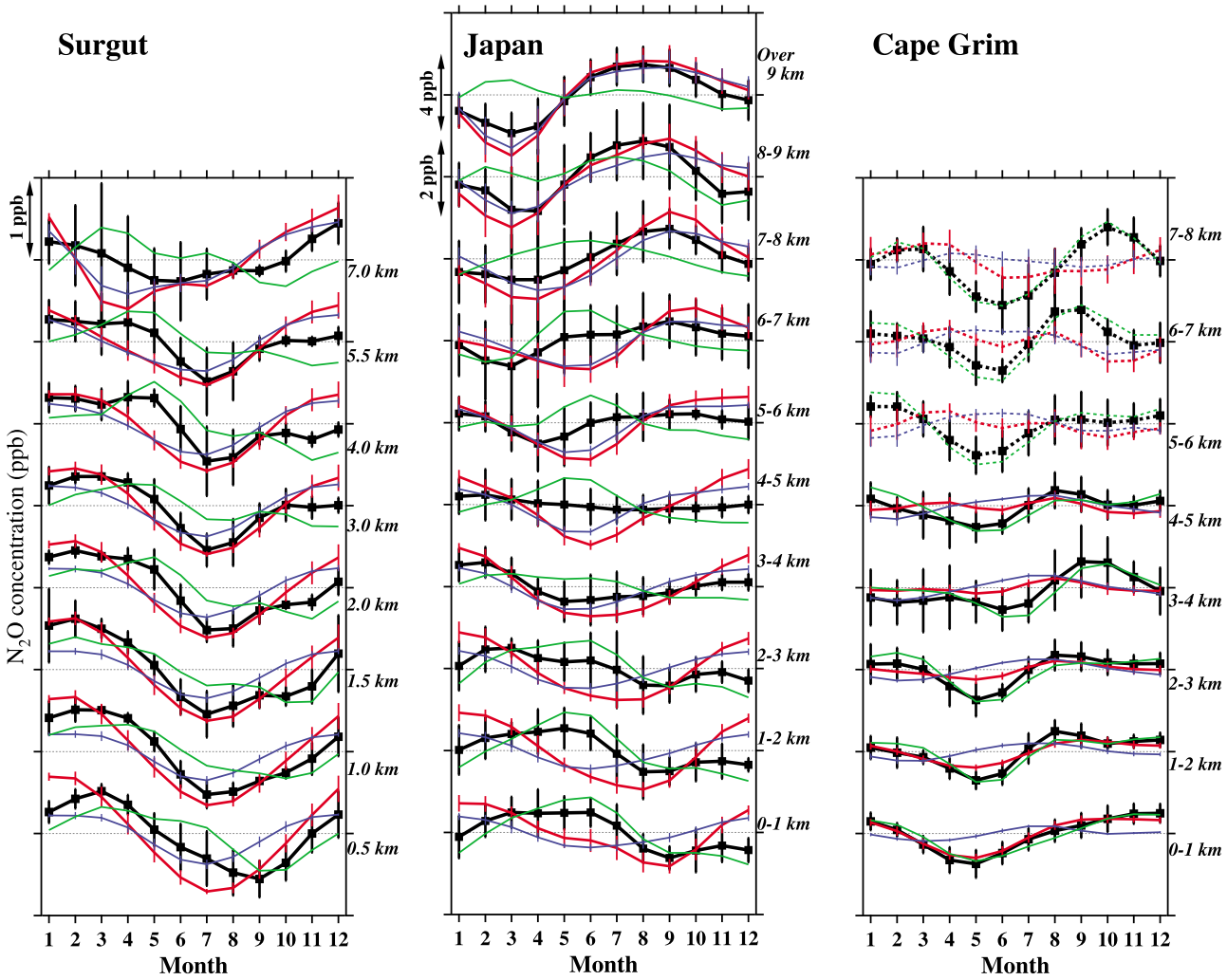

Figure 7. Mean seasonal cycles of N_2O concentration, detrended by the digital-filtering technique, over (left) Surgut, (middle) Japan, and (right) Cape Grim for each observation period (see text). Black and red lines represent results observed by aircraft and simulated by the ACTM, respectively. Blue lines represent the stratospheric contribution estimated from stratospheric tracer simulations. The green lines are the result obtained by subtracting the blue line from the black line (black minus blue): defined as the tropospheric contribution. Error bars represent 1 standard deviation for each monthly mean. In each panel, one division on the vertical axis indicates 1 ppb, except for two cases as follows: 2 ppb and 4 ppb at 8–9 km and over 9 km over Japan, respectively. Results above 5 km over Cape Grim are indicated by dashed lines because their statistical reliabilities are relatively low due to sparse data.

this site, although model N_2O resides within the observed variability as seen from the error bars. The raw observation data frequently show low concentrations during the spring, reflected in the large error bars specifically for this season.

[32] At 0.5 km altitude, the seasonal minimum is observed in September, while the model predicts a July minimum, suggesting that the ACTM is unable to represent the seasonal variation in the local-regional fluxes appropriately. In addition to the seasonal flux variability, the temporal variability of planetary boundary layer (PBL) height at Surgut is also significant. The ACTM simulated PBL height mostly exceeds 1000 m in the daytime in summer, while the PBL height mostly remains below 500 m in winter. Therefore, the 0.5 km altitude tends to be directly affected by local N_2O sources in summer. Additionally, the emission is enhanced in summer compared to winter. Such properties are reflected in larger error bars for observations at 0.5 km during the summer season (June–August), and also agree well with the estimated tropospheric contribution (green line) variation, which is obtained by subtracting the stratospheric contribution (blue line) from the observed seasonal cycle (black line).

3.3.2. N_2O Seasonal Cycles Over Japan

[33] Over Japan, large stratospheric effects producing minima in spring are pronounced in observation and ACTM results over 8 km. Seasonal amplitude in observations reaches 1.7 and 3.3 ppb at 8–9 km and over 9 km, respectively. The ACTM well reproduces their minima in spring, but overestimates the amplitudes by 20–30%. Interestingly, the month of the minimum in the stratospheric contribution looks to be shifting from spring to summer with decreasing altitude between 9 and 3 km (as more clearly seen in

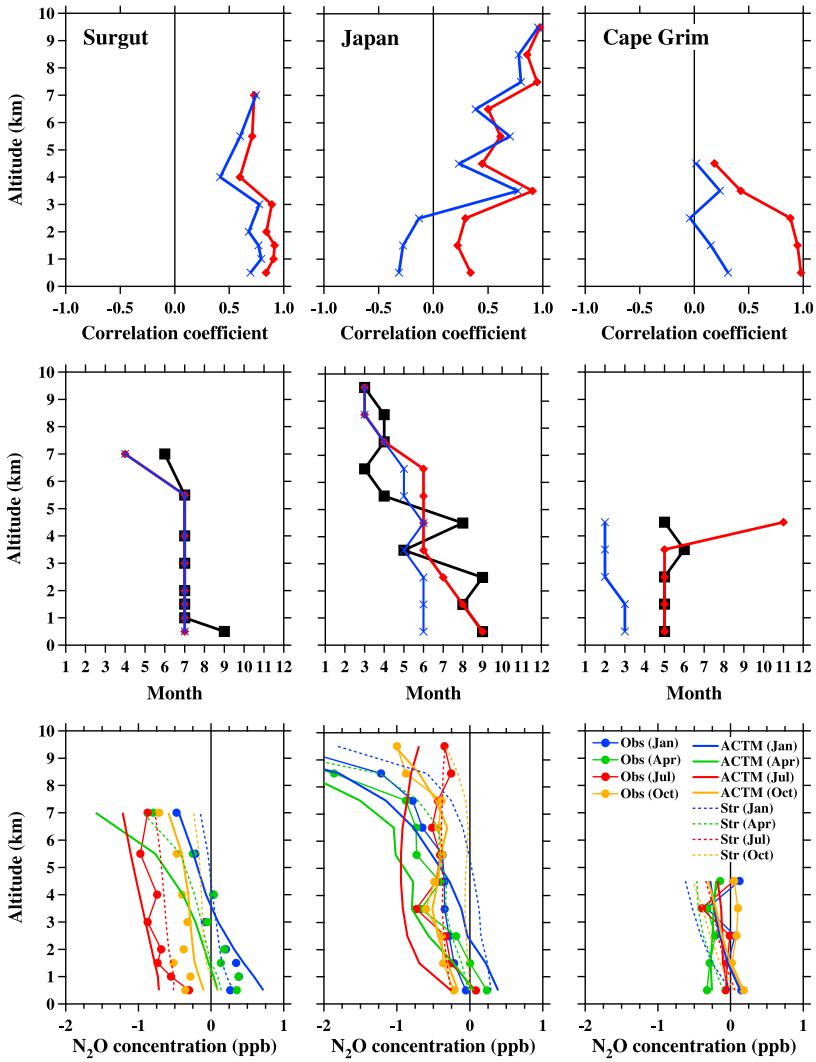

Figure 8. (top) For the three sites Surgut, Japan, and Cape Grim, shown are the altitude variation of the correlation coefficient between the measured N_2O seasonal cycle and the seasonal cycle simulated by the ACTM (red), and the seasonal cycle of the stratospheric contribution calculated by the ACTM (blue). (middle) For the same three sites, shown are the altitude variation of the month of the seasonal cycle minimum found from the measurements (black), and as simulated by the ACTM (red), as well as the month of the modeled minimum stratospheric contribution (blue). (bottom) Monthly mean vertical profiles of N_2O concentration observed (Obs) and simulated by the ACTM (ACTM), and the stratospheric contribution (Str) for January, April, July, and October are also shown, for the same three sites. The monthly means are calculated from their fitted curves, and adjusted so that their annual means are zero at the lowermost observation altitudes. Results above 5 km over Cape Grim are not shown for the same reason as that given for Figure 7.

Figure 8), which is different from that over Surgut (no shift between 1.0 and 5.5 km). This probably comes about from different transport pathways of the stratospheric influence. Over Japan, the stratospheric N_2O-depleted air propagates downward in the troposphere, after intruding at the tropopause just over Japan where the STE is very active as seen in Figure 6. Another interesting point is that the tropospheric contribution maximizes in early summer at lower altitudes. They probably reflect the seasonality of local surface fluxes. East Asia is the highest agricultural emission area in the world, especially after 2000, as reported in the recent EDGAR database (version 4, http://edgar.jrc.ec.europa.eu/). The sources can intensify due to application of fertilizer and/or weather factors such as high temperature and much precipitation in early summer. These competing contributions from both the stratosphere and local surface fluxes are likely responsible for N_2O seasonal cycles over Japan. We think that the ACTM fails to reproduce the observed seasonality below 7 km due to the lack of seasonality in the land fluxes in our simulations.

3.3.3. N_2O Seasonal Cycles Over Cape Grim

[34] Over Cape Grim, the ACTM well captures the observations below 3 km, where the stratospheric contributions are very weak. This indicates that the N_2O con-

centration over Cape Grim is dominantly controlled by the Southern Oceanic fluxes, taking into account that the oceanic flux is the only one that has seasonality in our simulations. This result is consistent with that of *Nevison et al.* [2005], who found seasonal N_2O outgassing from the Southern Ocean is important, and that the land source is almost negligible for the atmospheric N_2O seasonal cycle at Cape Grim (at the surface). Agreements between observations (black line) and the tropospheric contributions (green line) arise from very small stratospheric contributions over Cape Grim (blue line). We would like to avoid interpreting the results above 5 km (shown by dashed lines in Figure 7), because the observation data for the higher altitude levels are so sparse [*Francey et al.*, 1999], such that there is a high possibility for the derived seasonal cycle being artificial.

3.3.4. Vertical Profiles of Seasonal Cycle Correlation, Month of Minimum, and Annual Mean

[35] Figure 8 summarizes model-observation comparison results of vertical profiles of N_2O seasonal cycles for three aircraft observation sites. The correlations between observations and ACTM results indicate that stratospheric influence and vertical mixing by convection are significant for the summertime minima and the vertical uniformity throughout the troposphere over Surgut. Over Japan, there are both strong regional emissions and the stratospheric influence, and they seem to compete with each other in the middle troposphere. The former and the latter are dominant near the surface and in the free troposphere for N_2O seasonal cycles over Japan, respectively. No significant correlation between the observed N_2O seasonal cycle and the stratospheric contribution is seen over Cape Grim, in contrast to the strong correlations between ACTM results and observations below 3 km.

[36] Such vertical structures for individual sites are also reflected in the month of minimum concentration in the seasonal cycles. It is surprising that for the altitude range of 1.0 to 5.5 km over Surgut, the seasonal minimum in the observations, the ACTM simulation, and the simulated stratospheric contribution all occur in July. This is in contrast with the seasonal minimum being earlier at 7.0 km altitude, and later at 0.5 km altitude, although the ACTM shows no delay at 0.5 km. Over Japan, the month of minimum is delayed downward, i.e., from February at the uppermost altitude to September at the lowermost altitude for both observation and ACTM. The stratospheric contribution is also delayed by 3 months. This is a very different feature from that over Surgut. The discrepancy below 4 km over Japan is possibly due to local emissions. These differences in results over two sites in the Northern Hemisphere can be attributed to the atmospheric circulation in the Northern Hemisphere as well as differences in regional emissions. Over Cape Grim, the month of the seasonal minimum of the stratospheric contribution does not agree with that of the observation or simulation below 5 km, and the stratospheric influences are relatively weak, compared with the amplitudes over Surgut and Japan. Meanwhile below 3 km, the ACTM (red lines) can well reproduce the observations. In our simulation, only the oceanic flux has seasonality, exhibiting greater ventilation in the second half of the year in ocean areas south of Cape Grim. The seasonality of the oceanic flux is consistent with observation and model results below 3 km (Figure 7 [see also *Nevison et al.*, 2005]).

[37] The N_2O concentration generally decreases with altitude, but the rate of decrease varies significantly as a result of the seasonality in vertical transport and surface emissions. Figure 8 (bottom) shows the seasonal variations in N_2O vertical gradients as observed and simulated by the ACTM. Over Surgut, the observations show a steep decrease in lower altitudes (in PBL) and small gradients in the free troposphere in July because of the enhanced surface emissions and well-mixed middle troposphere (MT) due to increased convective activity, respectively. During the winter, when the vertical transport is weaker compared to the summer, vertical gradients can be seen at all sites in the MT region both in observations and ACTM. N_2O profiles over Japan in the UT region show large gradients due to stratospheric air intrusions in winter to spring, which are also well captured by the ACTM. The profiles can be separated into three parts: 1. LT region (<4 km), with the concentration decreasing with altitude, affected by surface sources, 2. MT region (4–7 km), with fairly uniform concentration, and 3. UT region, with large decreasing gradient (>7 km), highly affected by stratospheric air.

4. Conclusion

[38] The CCSR/NIES/FRCGC AGCM-based chemistry transport model (ACTM) has been developed for N_2O simulation in the troposphere-stratosphere height region. ACTM simulations have been performed for the period 1979–2008. We have validated our model for N_2O concentration variations in the troposphere and stratosphere by comparing it with several sets of aircraft observations and satellite observations from Aura-MLS, respectively. Comparisons with Aura-MLS observations suggest that the respective N_2O transport to the Northern and Southern Hemisphere during July–October and January–April can be successfully tracked by the ACTM, and the N_2O concentration gradient with altitude is reproduced within the uncertainty of MLS data (~15%). The ACTM simulation generally showed good agreement with observations in the UT/LS region. The stratospheric contributions to tropospheric N_2O variations have been studied by employing a stratospheric tracer method. These results indicate that N_2O seasonal cycles are significantly affected by the stratosphere-troposphere exchange in the upper troposphere region and subsequent mixing of the stratospheric N_2O-depleted air in the middle troposphere, and by the surface fluxes near the surface. The seasonality in tropospheric transport plays a significant role to convey the N_2O-depleted air and thus affect the N_2O seasonal cycles in the troposphere.

[39] Further detailed analysis using CONTRAIL-ASE data in the UT/LS region shows that the ACTM successfully captures each low N_2O concentration event in the UT during spring, which is caused by the intrusion of N_2O-depleted stratospheric air. High correlation coefficients (mostly > 0.8) between the CONTRAIL-ASE observations and the ACTM results indicate that the horizontal resolution of our model (T42: ~2.8 × 2.8°) is almost satisfactory to estimate the influence of STE on the global N_2O budget, but not enough

for precisely reproducing STE processes in particular around the strong concentration gradient with latitude at about 25°N/S where the correlation coefficients drops to ~0.6.

[40] Using vertical profile observations by aircraft at three sites, we have estimated influences of the stratosphere and of the troposphere on seasonal cycles of atmospheric N_2O concentration. N_2O seasonal cycles over Surgut in observation, ACTM and the stratospheric contribution show minima in the same month (July), at altitudes of 1.0–5.5 km. The results indicate that N_2O seasonal cycles over Surgut are mainly driven by the dilution of N_2O due to the stratospheric air propagation and relatively stronger vertical mixing by convection in summer than in winter. Over Japan, downward propagation of the stratospheric air and contribution of surface fluxes seem to be important in the free troposphere and near the surface, respectively. By contrast, over Cape Grim the results indicate that there is almost no stratospheric influence, and the seasonal variations are dominated by oceanic N_2O emissions.

[41] Discrepancies between observations and simulations near the surface in the Northern Hemisphere have indicated that more precise estimations of the seasonal variation in surface N_2O fluxes are needed. Inverse modeling, in which the influence of STE on surface N_2O is reasonably quantified by the model, would be capable of that. However, the fluxes might need to be expressed as a function of STE rate depending on the model, since there still seem to be uncertainties in the modeled STE at the present stage.

[42] **Acknowledgments.** We are grateful to the MLS/NASA teams for making the N_2O observations available at the Goddard Earth Sciences and Data Information Services Center (GES-DISC; http://daac.gsfc.nasa.gov). We also thank A.F. Bouwman for providing GEIA monthly flux data. Thanks go to Roger Francey of CAWCR/CSIRO for his long-term support of the vertical profile flights above Cape Grim. We extend our thanks to three anonymous reviewers for their helpful comments. This study was partly supported by the Grant-in-Aids for Young Scientists (B) (19710025) and for Creative Scientific Research (2005/17GS0203) of the Ministry of Education, Science, Sports and Culture, Japan.

References

Aoki, S., T. Nakazawa, T. Machida, S. Sugawara, S. Morimoto, G. Hashida, T. Yamanouchi, K. Kawamura, and H. Honda (2003), Carbon dioxide variations in the stratosphere over Japan, Scandinavia and Antarctica, *Tellus, Ser. B*, *55*, 178–186.

Appenzeller, C., J. R. Holton, and K. H. Rosenlof (1996), Seasonal variation of mass transport across the tropopause, *J. Geophys. Res.*, *101*(D10), 15,071–15,078, doi:10.1029/96JD00821.

Baray, J. L., V. Daniel, G. Ancellet, and B. Legras (2000), Planetary-scale tropopause folds in the southern subtropics, *Geophys. Res. Lett.*, *27*(3), 353–356, doi:10.1029/1999GL010788.

Bouwman, A. F., I. Fung, E. Matthews, and J. John (1993), Global analysis of the potential for N_2O production in natural soils, *Global Biogeochem. Cycles*, *7*, 557–597, doi:10.1029/93GB01186.

Bouwman, A. F., K. W. Van der Hoek, and J. G. J. Olivier (1995), Uncertainties in the global source distribution of nitrous oxide, *J. Geophys. Res.*, *100*(D2), 2785–2800, doi:10.1029/94JD02946.

Butler, J. H., J. W. Elkins, T. M. Thompson, and K. B. Egan (1989), Tropospheric and dissolved N_2O of the West Pacific and East Indian oceans during the El Niño Southern Oscillation event of 1987, *J. Geophys. Res.*, *94*(D12), 14,865–14,877, doi:10.1029/JD094iD12p14865.

Crutzen, P. J. (1970), The influence of nitrogen oxide on the atmospheric ozone content, *Q. J. R. Meteorol. Soc.*, *96*, 320–325, doi:10.1002/qj.49709640815.

Elbern, H., J. Hendricks, and A. Ebel (1998), A climatology of tropopause folds by global analyses, *Theor. Appl. Climatol.*, *59*, 181–200, doi:10.1007/s007040050023.

Forster, P., et al. (2007), Changes in atmospheric constituents and in radiative forcing, in *Climate Change 2007, The Physical Science Basis. Contribution of Working Group I to the Fourth Assessment Report of the Intergovernmental Panel on Climate Change*, edited by S. Solomon et al., pp. 129–234, Cambridge Univ. Press, Cambridge, U. K.

Francey, R. J., L. P. Steele, R. L. Langenfelds, and B. C. Pak (1999), High precision long-term monitoring of radiatively active and related trace gases at surface sites and from aircraft in the Southern Hemisphere atmosphere, *J. Atmos. Sci.*, *56*, 279–285, doi:10.1175/1520-0469(1999)056<0279:HPLTMO>2.0.CO;2.

Francey, R. J., et al. (2003), The CSIRO (Australia) measurement of greenhouse gases in the global atmosphere, in *Baseline Atmospheric Program Australia: 1999–2000*, edited by N. W. Tindale, N. Derek, and P. J. Fraser, pp. 42–53, Bur. of Meteorol., Melbourne, Victoria, Australia.

Hirsch, A. I., A. M. Michalak, L. M. Bruhwiler, W. Peters, E. J. Dlugokencky, and P. P. Tans (2006), Inverse modeling estimates of the global nitrous oxide surface flux from 1998–2001, *Global Biogeochem. Cycles*, *20*, GB1008, doi:10.1029/2004GB002443.

Holton, J. R., P. H. Haynes, M. E. Mcintyre, A. R. Douglass, R. B. Rood, and L. Pfister (1995), Stratosphere-troposphere exchange, *Rev. Geophys.*, *33*(4), 403–439, doi:10.1029/95RG02097.

Huang, J., et al. (2008), Estimation of regional emissions of nitrous oxide from 1997 to 2005 using multinetwork measurements, a chemical transport model, and an inverse method, *J. Geophys. Res.*, *113*, D17313, doi:10.1029/2007JD009381.

Ishijima, K., T. Nakazawa, S. Sugawara, S. Aoki, and T. Saeki (2001), Concentration variations of tropospheric nitrous oxide over Japan, *Geophys. Res. Lett.*, *28*(1), 171–174, doi:10.1029/2000GL011465.

Ishijima, K., T. Nakazawa, S. Sugawara, and S. Aoki (2009), Variations of atmospheric nitrous oxide concentration in the northern and western Pacific, *Tellus, Ser. B*, *61*, 408–415, doi:10.1111/j.1600-0889.2008.00406.x.

Jiang, X., W. L. Ku, R. L. Shia, Q. Li, J. W. Elkins, R. G. Prinn, and Y. L. Yung (2007), Seasonal cycle of N_2O: Analysis of data, *Global Biogeochem. Cycles*, *21*, GB1006, doi:10.1029/2006GB002691.

Jin, J. J., et al. (2009), Comparison of CMAM simulations of carbon monoxide (CO), nitrous oxide (N_2O), and methane (CH_4) with observations from Odin/SMR, ACE-FTS, and Aura/MLS, *Atmos. Chem. Phys.*, *9*, 3233–3252, doi:10.5194/acp-9-3233-2009.

Jones, R. L., and J. L. Pyle (1984), Observations of CH_4 and N_2O by the Nimbus-7 SAMS: A comparison with in-situ data and two-dimensional numerical model calculations, *J. Geophys. Res.*, *89*(D4), 5263–5279, doi:10.1029/JD089iD04p05263.

Kanamitsu, M., W. Ebisuzaki, J. Woolen, J. Potter, and M. Fiorino (2002), NCEP/DOE AMIP-II Reanalysis (R-2), *Bull. Am. Meteorol. Soc.*, *83*, 1631–1643, doi:10.1175/BAMS-83-11-1631(2002)083<1631:NAR>2.3.CO;2.

Lambert, A., et al. (2007), Validation of the Aura Microwave Limb Sounder middle atmosphere water vapor and nitrous oxide measurements, *J. Geophys. Res.*, *112*, D24S36, doi:10.1029/2007JD008724.

Levin, I., et al. (2002), Three years of trace gas observations over the EuroSiberian domain derived from aircraft sampling—A concerted action, *Tellus, Ser. B*, *54*, 696–712, doi:10.1034/j.1600-0889.2002.01352.x.

Liang, Q., A. R. Douglass, B. N. Duncan, R. S. Stolarski, and J. C. Witte (2009), The governing processes and timescales of stratosphere-to-troposphere transport and its contribution to ozone in the Arctic troposphere, *Atmos. Chem. Phys.*, *9*, 3011–3025, doi:10.5194/acp-9-3011-2009.

Liao, T., C. D. Camp, and Y. L. Yung (2004), The seasonal cycle of N_2O, *Geophys. Res. Lett.*, *31*, L17108, doi:10.1029/2004GL020345.

Machida, T., et al. (2001), Temporal and spatial variations of atmospheric CO_2 mixing ratio over Siberia, paper presented at Sixth International CO_2 Conference, World Meteorol. Org., Sendai, Japan.

Machida, T., H. Matsueda, Y. Sawa, Y. Nakagawa, K. Hirotani, N. Kondo, K. Goto, K. Ishikawa, T. Nakazawa, and T. Ogawa (2008), Worldwide measurements of atmospheric CO_2 and other trace gas species using commercial airlines, *J. Atmos. Oceanic Technol.*, *25*(10), 1744–1754, doi:10.1175/2008JTECHA1082.1.

Matsueda, H., T. Machida, Y. Sawa, Y. Nakagawa, K. Hirotani, H. Ikeda, N. Kondo, and K. Goto (2008), Evaluation of atmospheric CO_2 measurements from new flask air sampling of JAL airliner observations, *Pap. Meteorol. Geophys.*, *59*, 1–17, doi:10.2467/mripapers.59.1.

Muramatsu, H., T. Sasaki, M. Hirota, and Y. Makino (1984), An aircraft observation of an intrusion process of stratospheric ozone into the troposphere, *Pap. Meteorol. Geophys.*, *35*, 1–10, doi:10.2467/mripapers.35.1.

Nakazawa, T., and S. Sugawara (1997), Aircraft measurements of the concentrations of CO_2, CH_4, N_2O, and CO and the carbon and oxygen

isotopic ratios of CO_2 in the troposphere over Russia, *J. Geophys. Res.*, *102*(D3), 3843–3859, doi:10.1029/96JD03131.

Nakazawa, T., S. Morimoto, S. Aoki, and M. Tanaka (1993), Time and space variations of the carbon isotopic ratio of tropospheric carbon dioxide over Japan, *Tellus, Ser. B*, *45*, 258–274, doi:10.1034/j.1600-0889.1993.t01-2-00004.x.

Nakazawa, T., M. Ishizawa, K. Higuchi, and N. B. A. Trivett (1997), Two curve fitting methods applied to CO_2 flask data, *Environmetrics*, *8*, 197–218, doi:10.1002/(SICI)1099-095X(199705)8:3<197::AID-ENV248>3.0.CO;2-C.

Nevison, C. D., R. F. Weiss, and D. J. Erickson III (1995), Global oceanic emissions of nitrous oxide, *J. Geophys. Res.*, *100*(C8), 15,809–15,820, doi:10.1029/95JC00684.

Nevison, C. D., D. E. Kinnison, and R. F. Weiss (2004), Stratospheric influence on the tropospheric seasonal cycles of nitrous oxide and chlorofluorocarbons, *Geophys. Res. Lett.*, *31*, L20103, doi:10.1029/2004GL020398.

Nevison, C. D., R. F. Keeling, R. F. Weiss, B. N. Popp, X. Jin, P. J. Fraser, L. W. Porter, and P. G. Hess (2005), Southern Ocean ventilation inferred from seasonal cycles of atmospheric N_2O and O_2/N_2 at Cape Grim, Tasmania, *Tellus, Ser. B*, *57*, 218–229, doi:10.1111/j.1600-0889.2005.00143.x.

Nevison, C. D., N. M. Mahowald, R. F. Weiss, and R. G. Prinn (2007), Interannual and seasonal variability in atmospheric N_2O, *Global Biogeochem. Cycles*, *21*, GB3017, doi:10.1029/2006GB002755.

Numaguti, A., M. Takahashi, T. Nakajima, and A. Sumi (1997), Development of CCSR/NIES Atmospheric General Circulation Model, *CGER's Supercomput. Monogr. Rep. 3*, pp. 1–48, Natl. Inst. for Environ. Stud., Tsukuba, Japan.

Olivier, J. G. J., J. A. Van Aardenne, F. Dentener, L. Ganzeveld, and J. A. H. W. Peters (2005). Recent trends in global greenhouse gas emissions: Regional trends and spatial distribution of key sources, in *Non-CO_2 Greenhouse Gases (NCGG-4)*, edited by A. van Amstel, pp. 325–330, Millpress, Rotterdam, Netherlands.

Onogi, K., et al. (2007), The JRA-25 Reanalysis, *J. Meteorol. Soc. Jpn.*, *85*, 369–432, doi:10.2151/jmsj.85.369.

Patra, P. K., et al. (2008), TransCom model simulations of hourly atmospheric CO_2: Analysis of synoptic-scale variations for the period 2002–2003, *Global Biogeochem. Cycles*, *22*, GB4013, doi:10.1029/2007GB003081.

Patra, P. K., M. Takigawa, G. S. Dutton, K. Uhse, K. Ishijima, B. R. Lintner, K. Miyazaki, and J. W. Elkins (2009a), Transport mechanisms for synoptic, seasonal and interannual SF_6 variations and "age" of air in the troposphere, *Atmos. Chem. Phys.*, *9*, 1209–1225, doi:10.5194/acp-9-1209-2009.

Patra, P. K., et al. (2009b), Growth rate, seasonal, synoptic, diurnal variations and budget of methane in the lower atmosphere, *J. Meteorol. Soc. Jpn.*, *87*, 635–663, doi:10.2151/jmsj.87.635.

Potter, C. S., P. A. Matson, P. M. Vitousek, and E. A. Davidson (1996), Process modeling of controls on nitrogen trace gas emissions from soils world-wide, *J. Geophys. Res.*, *101*(D1), 1361–1377, doi:10.1029/95JD02028.

Prinn, R., D. Cunnold, R. Rasmussen, P. Simmonds, F. Alyea, A. Crawford, P. Fraser, and R. Rosen (1990), Atmospheric emissions and trends of nitrous oxide deduced from 10 years of ALE-GAGE data, *J. Geophys. Res.*, *95*(D11), 18,369–18,385, doi:10.1029/JD095iD11p18369.

Prinn, R. G., et al. (2000), A history of chemically and radiatively important gases in air deduced from ALE/GAGE/AGAGE, *J. Geophys. Res.*, *105*(D14), 17,751–17,792, doi:10.1029/2000JD900141.

Ravishankara, A. R., J. S. Daniel, and R. W. Portmann (2009), Nitrous oxide (N_2O): The dominant ozone-depleting substance emitted in the 21st century, *Science*, *326*, 123-125, doi:10.1126/science.1176985.

Sander, S. P., et al. (2006), Chemical kinetics and photochemical data for use in atmospheric studies: Evaluation number 15, *JPL Publ. 06–2*, Jet Propul. Lab., Calif. Inst. of Technol., Pasadena.

Schuck, T. J., C. A. M. Brenninkmeijer, A. K. Baker, F. Slemr, P. F. J. van Velthoven, and A. Zahn (2010), Greenhouse gas relationships in the Indian summer monsoon plume measured by the CARIBIC passenger aircraft, *Atmos. Chem. Phys. Discuss.*, *10*, 2031–2087, doi:10.5194/acpd-10-2031-2010.

Sekiguchi, M., and T. Nakajima (2008), A k-distribution-based radiation code and its computational optimization for an atmospheric general circulation model, *J. Quant. Spectrosc. Radiat. Transfer*, *109*, 2779-2793, doi:10.1016/j.jqsrt.2008.07.013.

Strong, K., et al. (2008), Validation of ACE-FTS N_2O measurements, *Atmos. Chem. Phys.*, *8*, 4759–4786, doi:10.5194/acp-8-4759-2008.

Sudo, K., and H. Akimoto (2007), Global source attribution of tropospheric ozone: Long-range transport from various source regions, *J. Geophys. Res.*, *112*, D12302, doi:10.1029/2006JD007992.

Takigawa, M., M. Takahashi, and H. Akiyoshi (1999), Simulation of ozone and other chemical species using a Center for Climate System Research/National Institute for Environmental Studies atmospheric GCM with coupled stratospheric chemistry, *J. Geophys. Res.*, *104*(D11), 14,003–14,018, doi:10.1029/1998JD100105.

Urban, J., et al. (2005), Odin/SMR limb observations of stratospheric trace gases: Validation of N_2O, *J. Geophys. Res.*, *110*, D09301, doi:10.1029/2004JD005394.

Weiss, R. F. (1981), The temporal and spatial distribution of tropospheric nitrous oxide, *J. Geophys. Res.*, *86*(C8), 7185–7195, doi:10.1029/JC086iC08p07185.

S. Aoki and T. Nakazawa, Center for Atmospheric and Oceanic Studies, Tohoku University, Sendai 980-8578, Japan.

K. Ishijima, P. K. Patra, and M. Takigawa, Environmental Biogeochemical Cycle Research Program, Research Institute for Global Change, Japan Agency for Marine-Earth Science and Technology, 3173-25 Showamachi, Kanazawa, Yokohama, Kanagawa 236-0001, Japan. (ishijima@jamstec.go.jp)

P. B. Krummel, R. L. Langenfelds, and P. Steele, Centre for Australian Weather and Climate Research, CSIRO Marine and Atmospheric Research, Aspendale, Vic 3195, Australia.

T. Machida, Global Environmental Research Center, Tsukuba, Ibaraki 305-8506, Japan.

H. Matsueda and Y. Sawa, Geochemical Research Department, Meteorological Research Institute, Tsukuba, Ibaraki 305-0052, Japan.